CHEMICAL ENGINEERING TRANSACTIONS
VOL. 47, 2016
A publication of AIDIC
The Italian Association of Chemical Engineering
Online at www.aidic.it/cet
Guest Editors: Angelo Chianese, Luca Di Palma, Elisabetta Petrucci, Marco Stoller

ISBN 978-88-95608-38-9; **ISSN** 2283-9216
DOI: 10.3303/CET1647015

Formation of Hematite Nanotubes by Two-Step Electrochemical Anodization for Efficient Degradation of Organic Pollutants

Bianca Lucas-Granados, Rita Sánchez-Tovar, Ramón M. Fernández-Domene, José García-Antón*

Grupo de Ingeniería Electroquímica y Corrosión (IEC). Instituto de Seguridad Industrial, Radiofísica y Medioambiental (ISIRYM). Universitat Politècnica de València. Valencia. Spain.
jgarciaa@iqn.upv.es

Nowadays, hematite (α-Fe_2O_3) has emerged as a promising photocatalyst for efficient degradation of organic pollutants due to its properties such as suitable band-gap (~2.1 eV), stability against photocorrosion, abundance and low cost. However, some drawbacks such as low carrier mobility and short hole diffusion length limit its efficiency. In order to overcome these issues, self-ordered nanotubes can be synthetized. Anodization is one of the simplest and most economic techniques to produce nanostructures with high control. In the present study, self-ordered hematite nanotubes were synthetized by two-step electrochemical anodization. In two-step anodization, a first-step was actually a pretreatment to form well-ordered nanoporous template in which well-ordered nanotubes are grown by a second-step. The formed nanotubes were characterized by different methods such as Field Emission Scanning Microscopy and Raman spectroscopy to determine their morphology and crystalline structure, respectively. Furthermore, the obtained nanotubes were characterized by means of photocurrent density versus potential measurements (water splitting) to evaluate their efficiency as photocatalyst. Good results were obtained as the achieved photocurrent density was 0.079 mA cm^{-2} at 0.58 V (vs. Ag/AgCl), which indicates that the nanotubes synthetized by two-step anodization are suitable photocatalysts for degradation of organic pollutants.

1. Introduction

Iron oxide in its hematite crystalline structure is an interesting material for being used as photocatalyst for efficient degradation of organic pollutants as it possesses advantageous properties such as suitable band-gap (~2.1 eV), electrochemical stability, low toxicity and abundance (De Carvalho et al., 2012). Nevertheless, its low carrier mobility, short lifetime of the excited-state carriers (10^{-12} s) and short hole diffusion length limit its efficiency (Wang et al., 2014). The phocatalytic activity is mainly attributed to the generation of electron-hole pairs under illumination, and these holes are strong oxidizing agents. These holes can produce two reactions (Müller and Schmuki, 2014):
1. The holes can directly oxidize the organic compounds.
2. The holes can react with H_2O to form hydroxyl radicals (•OH) that act as oxidizing agents of the organic compounds.
Sivula et al. (2011) reported that the morphology control of the hematite structures in the scale of nanometers, can overcome some of the hematite drawbacks. Nano-dimensional semiconductor materials have innumerable applications because of their shape and size dependent properties (Souza et al., 2013). In the last years, the fabrication of nanostructures has attracted special interest for several applications like catalysis and electric power generation (Eftekhari, 2008; Piazza et al., 2013). Specially, vertically oriented nanotubes are considered interesting for photo-induced processes, as they improve the electron transport properties and provide longer electron lifetime, because the wall thickness of the nanotubes make the electron-hole recombination lower and it plays crucial role in photocatalytic reactions (Matarrese et al., 2014). Nanostructures of iron oxide have been synthetized by different methods such as sol-gel, thermal oxidation,

Please cite this article as: Lucas-Granados B., Sánchez-Tovar R., Fernández-Domene R.M., Garcia-Anton J., 2016, Formation of hematite nanotubes by two-step electrochemical anodization for efficient degradation of organic pollutants., Chemical Engineering Transactions, 47, 85-90 DOI: 10.3303/CET1647015

electrospinning, electrodeposition and electrochemical anodization. Among these techniques, electrochemical anodization has become attractive in recent years as it can form ordered nanotubular oxides with high surface area and low cost (Rangaraju et al., 2009). Some authors studied a new two-step anodization in order to form ordered nanotubes and they evaluated their application in photoelectrocatalytic degradation of azo dye (Zhang et al., 2010).

In the present study, we synthetized hematite nanotubes by two-step electrochemical anodization and compared them with hematite nanotubes synthetized by simple anodization. The aim of this study is to compare the nanotubes obtained by simple and two-step anodization and establish the better method to obtain a suitable photocatalyst for applications such as degradation of organic pollutants. For the morphological characterization we used Field Emission Scanning Electron Microscopy (FE-SEM) and for the crystallographic evaluation Raman spectroscopy. Photocurrent density versus time measurements were performed in order to evaluate the efficiency of the obtained nanostructures as photocatalysts.

2. Experimental procedure

2.1 Electrochemical two-step anodization

Anodization was carried out by using iron rods (99.9% purity) as working electrode and a platinum foil as counter electrode. Prior to anodization, iron rod surface was abraded with 220 to 4000 silicon carbide (SiC) papers in order to obtain a mirror finish. After this, iron samples were sonicated in ethanol during 2 minutes, washed with distilled water and dried in a nitrogen stream. Once the samples were cleaned, electrochemical anodization was performed in an ethylene glycol based solution containing 0.1 M ammonium fluoride (NH_4F) and 3%vol. water. The first step of the anodization was carried out at 50 V during 5 minutes, then the samples were sonicated in distilled water for 10 minutes and dried in nitrogen. After this, the second step of the anodization was performed with fresh solution at the same conditions (50 V for 5 minutes) and then, the samples were rinsed with distilled water and dried in nitrogen. Once the samples were anodized, annealing was carried out at 500 ^{O}C for 1 hour in air. The samples were cooled within the furnace by natural convection.

2.2 Characterization

The samples were characterized by different methods with the aim of evaluating its efficiency as photocatalyst for degradation of organic pollutants. Raman spectroscopy (using a 632 nm neon laser with ~700 μW) was used to evaluate the crystalline structure of the obtained nanostructures. FE-SEM was used to characterize the morphology of the nanostructure. Finally, photocurrent density versus applied potential under chopped light (water splitting) measurements were carried out to determine the efficiency of the obtained nanostructure as photocatalyst. Water splitting tests were performed in a three-electrode configuration using a platinum tip as counter electrode, a saturated Ag/AgCl (3 M KCl) as reference electrode and the synthetized iron oxide nanostructure as working electrode. The experiments were conducted in a photoelectrochemical cell with an area of 0.26 cm^2 exposed to the solution (KOH 1 M). Photocurrent density versus potential measurements were recorded by scanning the potential from -0.3 to + 0.7 V (vs. Ag/AgCl) by chopped light irradiation (0.02 V with illumination and 0.02 V in the dark) with a scan rate of 2 $m \cdot s^{-1}$. The tests were performed under simulating sunlight conditions AM 1.5 (100 $mW \cdot cm^{-2}$).

3. Results and discussion

Figure 1 shows a schematic representation of the steps carried out for the synthesis of the nanotubes. In the first step of the electrochemical anodization, random iron oxide nanotube arrays were formed. Then, the sonication during 10 minutes results in removing the formed nanotubes leaving the nanoporous as a template for the formation of self-ordered nanotubes during the second step of anodization. Finally, annealing was performed in order to transform the amorphous Fe_2O_3 into crystalline α-Fe_2O_3.

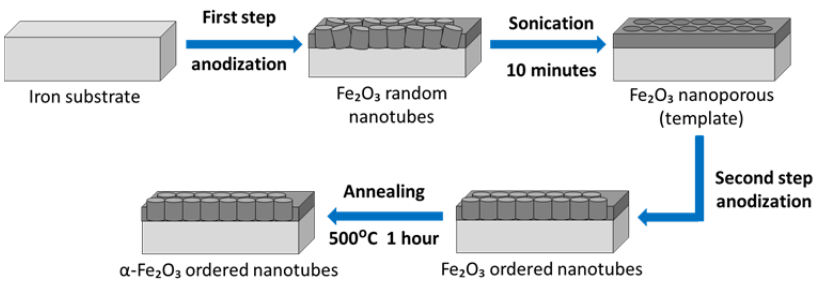

Figure 1: Schematic representation of the steps for the synthesis of α-Fe_2O_3 ordered nanotubes.

The first step of the electrochemical anodization for the formation of the nanotubes consists of two stages. Firstly, a compact oxide layer (Fe_2O_3) was formed according to Eq(1) and a quick drop of the current density was observed as shown in Figure 2, where the current density versus time during simple and two-step anodization is represented.

$$2Fe + 3H_2O \rightarrow Fe_2O_3 + 3H_2 \quad (1)$$

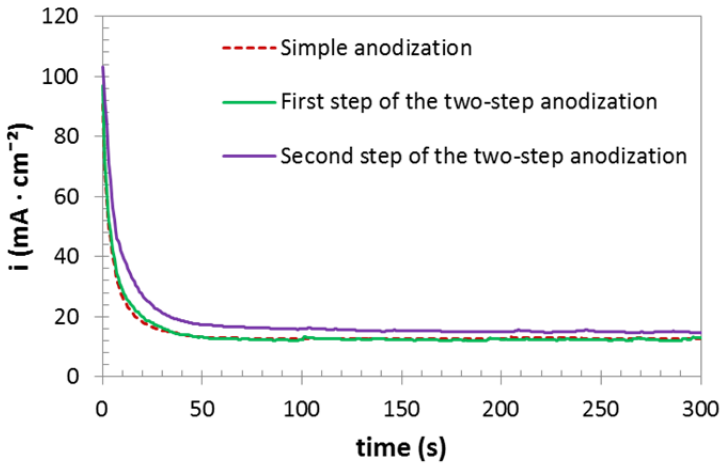

Figure 2: Current density versus time during both simple and two-step electrochemical anodization of iron at 50 V in an ethylene glycol containing 0.1M NH_4F and 3 %vol. water.

Then, the formation of tiny pits at the surface of the compact layer followed by the formation of nanoporous structure was produced. This process occurs because the presence of fluoride ions (F^-) combined with the applied potential leads to a partial dissolution of the compact Fe_2O_3 layer according to Eq(2). The last stage is the formation of the nanotubes due to further dissolution and cation-cation repulsion. This formation continues until equilibrium is reached between the formation of the oxide layer and the chemical dissolution by fluoride ions, and then the formation of the nanotubes stops (Mohapatra et al., 2009; Xie et al., 2014) and the photocurrent density remains almost constant as shows Figure 2.

$$Fe_2O_3 + 12F^- + 6H^+ \rightarrow 2[FeF_6]^{3-} + 3H_2O \quad (2)$$

Figure 2 shows that the first step achieves lower photocurrent densities than the second one. This is because the first step starts in the iron substrate whereas the second step starts in the nanoporous Fe_2O_3 array, so the latter step is faster and results in higher photocurrent density. Furthermore, as one can expect, the simple anodization curve is similar to the one for first step of the two-step anodization due to the fact that the simple anodization starts on iron substrate as the first step of the two-step anodization.

In Figure 3, FE-SEM views show the top (a) and c)) and cross sectional (b) and d)) images of the samples anodized by simple and two-step anodization, respectively. It can be seen that there are no significant differences in the morphology, as the views show nanotubular structure for both cases. Then, the two-step anodization does not affect the morphology in comparison with simple anodization but the differences are in the dimensions of this nanotubular structures. The nanotubular structure is beneficious for degradation of organic pollutants as when electron-holes are generated, the thin walls of the nanotubes allows the generated holes to move toward the surface and the tubular direction directly back contacted to the substrate allows the electron to move toward the substrate, then the recombination losses are minimized. In nanotubes the holes can reach the surface faster than in other nanoarchitectures and hence, can degrade the organic pollutants easier than in other nanostructures (Mohapatra et al., 2009).

Table 1 shows the values of inner diameters and lengths obtained for the nanostructures anodized by simple and two-step anodization. The inner diameters are higher for the two-step anodization whereas the length of the nanotubes is higher for the simple anodization.

On the one hand, the higher inner diameters may be related to the thinner walls of the nanotubes which result in better hole diffusion. On the other hand, the lower length in the samples anodized by two-step anodization is beneficious for the degradation of organic pollutants because a short nanotubular structure is considered to be favorable for the electron transport inside the electrode. Furthermore, the short length of the nanotubes contributes to a more mechanical stability of the electrode (Liu et al., 2009).

Table 1: FE-SEM measurements of the anodized samples.

Anodization	Inner diameter (nm)	Length (nm)
Simple	59 ± 10	747 ± 25
Two-step	88 ± 12	564 ± 18

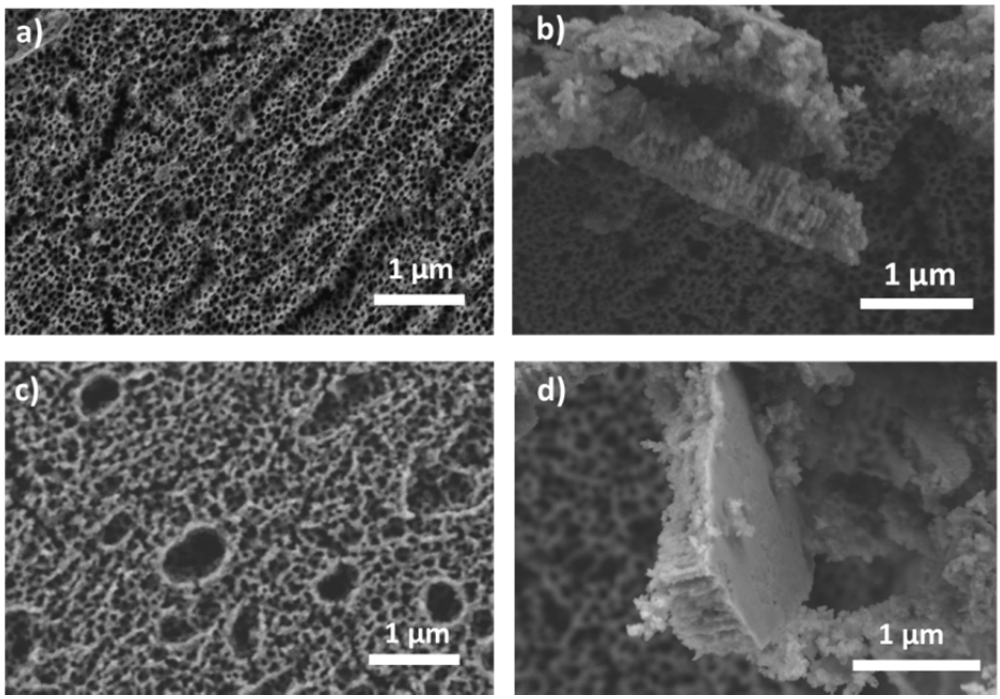

Figure 3: FE-SEM top(a)-c)) and cross sectional(b)-d)) images of the samples anodized by simple (a)-b)) and two-step (c)-d)) anodization at 50 V in an ethylene glycol containing 0.1M NH_4F and 3 %vol. water.

Figure 4 shows the crystalline phases determined by Raman microscopy for the samples annealed by simple and two-step anodization. The Raman spectra of the nanostructures show that the crystalline phase for both nanostructures is mainly hematite (α-Fe_2O_3). The peak that appears at 229 cm^{-1} is assigned to the A_{1g} mode of hematite and it appears for both samples anodized by simple and two-step anodization. Moreover, the peaks observed at 249 cm^{-1} (E_g), 295 cm^{-1} (E_g), 414 cm^{-1} (E_g), 500 (A_{1g}), 615 (E_g) and 1317 cm^{-1} (2_{nd} order) are also associated with the hematite structure and they appear for the nanostructures anodized by simple and two-step anodization, so both nanostructures are mainly composed by hematite. Additionally, a peak that appears at 672 cm^{-1} (T_{2g}) corresponds to the magnetite phase (Jubb et al., 2010; Nie et al., 2013). This indicates that although the predominant crystalline phase in both nanostructures is hematite (α-Fe_2O_3), a little amount of magnetite appears in the structure. This little amount of magnetite phase can enhance the conductivity of the nanostructures because of the electron and holes hopping between the Fe^{2+} and Fe^{3+} ions that are located at the octahedral sites in the inversed spinel structure of the magnetite. (Mettenbörger, 2014).

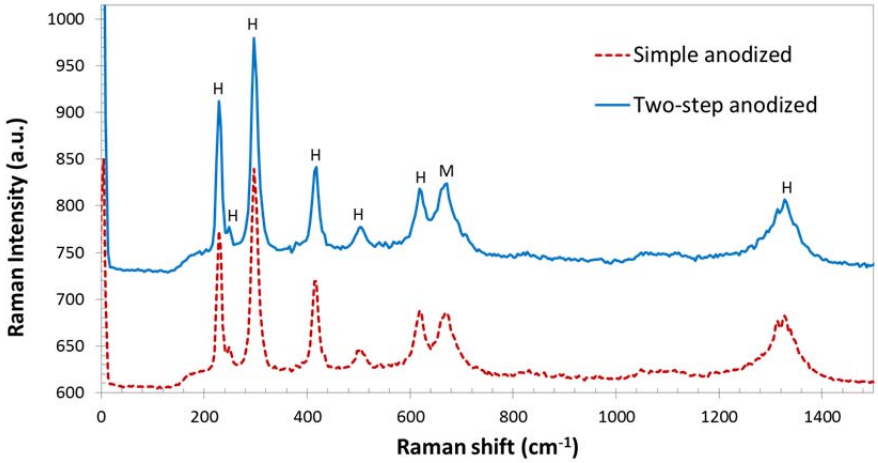

Figure 4: Raman spectra of the samples anodized by simple and two-step anodization at 50 V in an ethylene glycol solution containing 0.1M NH_4F and 3 %vol. water and annealed in air at 500 ^{O}C during 1 hour. H: Hematite, M: Magnetite.

Figure 5 shows the photocurrent density versus potential measurements that indicate the efficiency of the nanostructure as photocatalyst for degradation of organic pollutants. The nanostructure synthetized by two-step anodization show better performance than the one synthetized by simple anodization, achieving a photocurrent density of 0.079 mA cm^{-2} at 0.58 V vs. Ag/AgCl. This means that the sample synthetized by two-step anodization might be better photocatalyst for degradation of organic pollutants than the one anodized by simple anodization. This is in agreement with the FE-SEM measurements that indicated lower thickness for the samples anodized by two-step anodization that improve the hole diffusion and furthermore, the wider nanotubes might be less screened against light irradiation. This could enhance the photocurrent density indicating that the samples anodized by two-step anodization are good photocatalysts for degradation of organic pollutants.

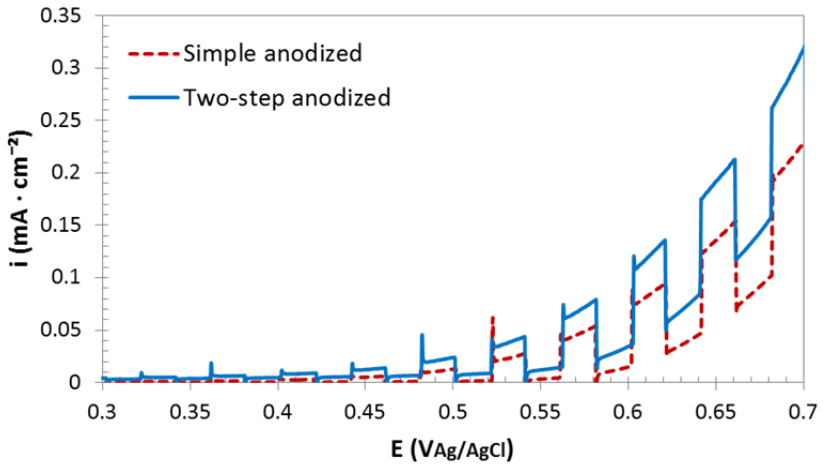

Figure 5: Photocurrent density versus potential measurements for the samples anodized by simple and two-step anodization at 50 V in an ethylene glycol solution containing 0.1M NH_4F and 3 %vol. water and annealed in air at 500 ^{O}C during 1 hour.

4. Conclusions

Our study has compared simple and two-step electrochemical anodization in order to evaluate the efficiency of the obtained nanostructures as photocatalysts for degradation of organic pollutants. The two-step anodization consists of making a template that allows the consequent growth of ordered nanotubes from the nanopores directly on the iron substrate. After annealing in certain conditions, the amorphous Fe_2O_3 nanostructure turns

into crystalline hematite (α-Fe_2O_3) with little amount of magnetite phase (Fe_3O_4) as revealed Raman spectroscopy, which allows the nanostructure to be used as photocatalyst.
Comparing simple and two-step anodization, the morphology of both nanostructures are similar as shows FE-SEM measurements. However, the two-step anodization obtained nanotubes with higher inner diameters which improve the photocatalytic activity because of the better hole diffusion against the walls of the nanotubes and the better irradiation of the nanostructure under simulated solar light. Hence, the good results of the photocurrent density versus potential measurements (0.079 mA $\cdot$ cm^{-2} at 0.58 V (vs. Ag/AgCl)) indicate that the obtained nanostructure synthetized by two-step anodization can be used as photocatalyst in applications such as degradation of organic pollutants.

Acknowledgments

The authors would like to express their gratitude for the financial support to the Ministerio de Economía y Competitividad (Reference: BES-2014-068713, Project Code: CTQ2013-42494-R), for its help in the Laser Raman Microscope acquisition (UPOV08-3E-012), and for the co-finance by the European Social Fund.

References

De Carvalho V. a N., Luz R. a de S., Lima B.H., Crespilho F.N., Leite E.R., Souza F.L., 2012, Highly oriented hematite nanorods arrays for photoelectrochemical water splitting, J. Power Sources, 205, 525–529, DOI:10.1016/j.jpowsour.2012.01.093

Eftekhari A., 2008, Nanostructured Materials in Electrochemistry. WILEY-VCH Verlag GmbH & Co. KGaA, Weinheim, Germany.

Jubb A.M., Allen H.C., 2010, Vibrational spectroscopic characterization of hematite, maghemite, and magnetite thin films produced by vapor deposition, ACS Appl. Mater. Interfaces 2, 2804–2812, DOI:10.1021/am1004943

Liu Y., Zhou B., Li J., Gan X., Bai J., Cai W., 2009, Preparation of short, robust and highly ordered TiO_2 nanotube arrays and their applications as electrode, Appl. Catal. B Environ. 92, 326–332, DOI:10.1016/j.apcatb.2009.08.011

Matarrese R., Nova I., Bassib A.L., Casarib C.S., Russob V., 2014, Hierarchical Nanostructured TiO_2 Films Prepared by Reactive Pulsed Laser Deposition for Photoelectrochemical Water Splitting, Chemical Engineering Transactions 41, 313–318, DOI:10.3303/CET1441053

Mettenbörger A., Singh T., Singh A.P., Järvi T.T., Moseler M., Valldor M., Mathur S., 2014, Plasma-chemical reduction of iron oxide photoanodes for efficient solar hydrogen production, Int. J. Hydrogen Energy 39, 4828–4835, DOI:10.1016/j.ijhydene.2014.01.080

Mohapatra S.K., John S.E., Banerjee S., Misra M., 2009, Water Photooxidation by Smooth and Ultrathin α-Fe_2O_3 Nanotube Arrays, Chem. Mater. 21, 3048–3055, DOI:10.1021/cm8030208

Müller V., Schmuki P., 2014, Efficient photocatalysis on hierarchically structured TiO_2 nanotubes with mesoporous TiO_2 filling, Electrochem. commun. 42, 21–25, DOI:10.1016/j.elecom.2014.01.018

Nie S., Starodub E., Monti M., Siegel D. a., Vergara L., El Gabaly F., Bartelt N.C., De La Figuera J., McCarty K.F., 2013, Insight into magnetite's redox catalysis from observing surface morphology during oxidation, J. Am. Chem. Soc. 135, 10091–10098, DOI:10.1021/ja402599t

Piazza S., Genduso G., Inguant, R., 2013, Nickel-Indium Sulphide Core-Shell Nanostructures obtained by Spray-ILGAR Deposition, Chemical Engineering Transactions 32, 2239–2244, DOI:10.3303/CET1332374

Rangaraju R.R., Panday a, Raja K.S., Misra M., 2009, Nanostructured anodic iron oxide film as photoanode for water oxidation, J. Phys. D. Appl. Phys. 42, 135303, DOI:10.1088/0022-3727/42/13/135303

Sivula K., Le Formal F., Grätzel M., 2011, Solar Water Splitting: Progress Using Hematite (α-Fe_2O_3) Photoelectrodes, ChemSusChem 4, 432–449, DOI:10.1002/cssc.201000416

Souza D. a R., Gusatti M., Sanches C., Moser V.M., Kuhnen N.C., Riella H.G., 2013, Initial studies of photocatalytic discolouration of methyl orange by using ZnO nanostructures, Chemical Engineering Transactions 32, 2275–2280, DOI:10.3303/CET1332380

Wang L., Lee C.Y., Schmuki P., 2014, Improved photoelectrochemical water splitting of hematite nanorods thermally grown on Fe-Ti alloys, Electrochem. commun. 44, 49–53, DOI:10.1016/j.elecom.2014.04.010

Xie K., Guo M., Huang H., Liu Y., 2014, Fabrication of iron oxide nanotube arrays by electrochemical anodization, Corros. Sci. 88, 66–75, DOI:10.1016/j.corsci.2014.07.019

Zhang, Z., Hossain, M.F., Takahashi, T., 2010, Self-assembled hematite (α-Fe2O3) nanotube arrays for photoelectrocatalytic degradation of azo dye under simulated solar light irradiation, Applied Catalysis B: Environmental 95, 423–429, DOI:10.1016/j.apcatb.2010.01.022